

## Bridging EUV and white-light observations using the *PROBA2/SWAP* imager and MLSO/MK4 coronagraph via advanced image processing methods: a ‘double eruption’ CME case study.

J. P. Byrne<sup>1</sup> · et al.

© Springer •••

**Abstract** Methods of multiscale image analysis were employed and their efficacy on the SWAP data tested for revealing CME structure while suppressing other features. The methods use successive filtering of an image via a Gaussian and derivative-of-Gaussian produces a number of scales of detail to be inspected. This also produces an image with intensities that represent the relative edge strengths in the original image, which can be used to characterize the structure of interest – specifically for this case the erupting material involved in the CME. In order to overlap the observations from SWAP and MK4, the core material of the CME in its early eruption phase was chosen for its higher signal to noise ratio than the CME front, for example, that was not discernible in the early stages of the observations. In the LASCO field-of-view, the core material was determined to be moving at the same speed as the CME front, at  $\sim 500 \text{ km s}^{-1}$ . The front portion of the core material in the MK4 images was characterized via point-&-click methodology on the multiscale images of enhanced edges, and an ellipse was fit to the curved front. The same was done for the erupting loop structure observed in SWAP, with the expectation that it might directly correlate to the CME core. However, it was found that the erupting material that starts at the same time and location in both the MK4 and SWAP images, did not proceed to erupt at the same rate. Rather the core material observed in MK4 moves at greater speeds than the loop structures observed in SWAP; rising from an initial speed of  $\sim 100 \text{ km s}^{-1}$  (at  $\sim 1.5 R_\odot$ ) to a final speed of  $\sim 400 \text{ km s}^{-1}$  (at  $\sim 2 R_\odot$ ), while the loops continue to steadily rise at  $\sim 100 \text{ km s}^{-1}$ . The reason for this is unclear, and requires further investigation.

**Keywords:** Coronal Mass Ejections, Initiation and Propagation

---

<sup>1</sup> Institute for Astronomy, University of Hawai'i, 2680 Woodlawn Drive, Honolulu, HI 96822, USA. email:  
jbyrne@ifa.hawaii.edu

## 1. Introduction

Coronal mass ejections (CMEs) represent the largest, most dynamic phenomena that originate from the Sun. Propagating at speeds of hundreds up to thousands of kilometers per second (Yashiro *et al.*, 2004), the particle densities and energies involved can cause adverse space weather at Earth and elsewhere in the heliosphere (Schwenn *et al.*, 2005). They can lead to geomagnetic storms upon impacting our magneto-sphere, damaging satellites, affecting communication and navigation systems, and increasing the radiation risk for astronauts (Lockwood and Hapgood, 2007). Given their potentially hazardous impact on Earth's geomagnetic environment, the physics governing their eruption and propagation needs to be understood.

An important aspect of studying CME initiation, is the ability to resolve their low-corona propagation and associated source regions on the disk: be it a flaring or non-flaring active region, a prominence/filament eruption or other rising loop system, or else a ‘stealth CME’ without any specifically detectable source. Prominence lift-offs often become the core material of a CME, and rising loops often form some part of the CME morphology. Their low-corona kinematics and morphology provide insight into the early forces at play, and so a rigorous study of such phenomena is key to understanding the physics involved.

In order to connect CMEs to their source regions, data from disk imagers such as the Sun Watcher using APS detectors and image Processing (SWAP; Seaton *et al.*, 2013) onboard the second Projects for Onboard Autonomy (*PROBA2*; Santandrea *et al.*, 2013) and the Atmospheric Imaging Assembly (AIA; Lemen *et al.*, 2012) onboard the Solar Dynamics Observatory (*SDO*; Pesnell, Thompson, and Chamberlin, 2012), may be used in tandem with coronagraph observations. However, difficulties in the interpretation of the observed features arise due to the varying instrument specifications, e.g., image passbands, fields-of-view, cadences, etc. Therefore, to bridge the gap between the white-light images of the extended corona and the EUV observations of the solar disk and low corona, the SWAP imager was used in conjunction with the Mauna Loa Solar Observatory (MLSO) MK4 coronagraph (Elmore *et al.*, 2003) to directly compare the observations of CMEs as they erupt through the overlapping fields-of-view (Fig. 1). This allows a direct correspondence of features in the EUV images with those in the white-light images, providing new insight into the connection of CMEs to the Sun during their initial phases of eruption and acceleration away from their source regions on the disk.

A difficulty exists in studies of coronal structure that are prone to low signal-to-noise ratios in the observational data. Low-coronal white-light observations using a coronagraph are problematic due to the strong radial brightness gradient and issues with scattered light in the instrument, while extended EUV disk observations are problematic due to the strong drop-off in emission brightness with increasing coronal height. These common issues with solar observational data motivate the development and use of advanced image processing techniques to suppress noise and enhance structures in the image data (Druckmüllerová, Morgan, and Habbal, 2011, Gallagher *et al.*, 2011, Pérez-Suárez *et al.*, 2011, Stenborg, Vourlidas, and Howard, 2008, Young and Gallagher, 2008, Morgan, Habbal, and Woo, 2006, Stenborg and Cobelli, 2003).

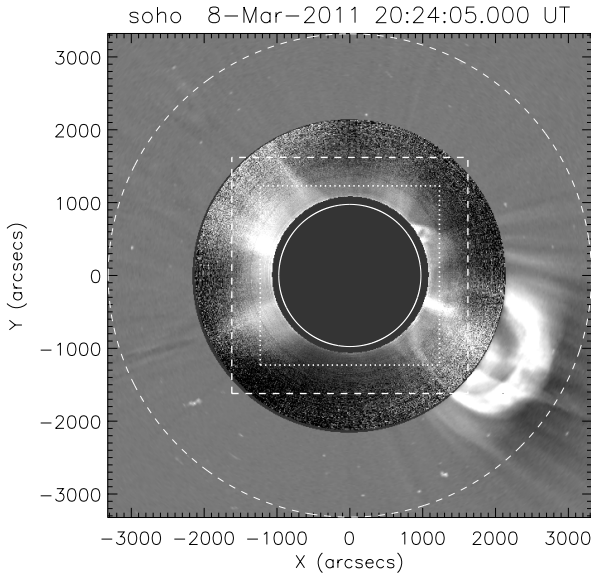


**Figure 1.** A LASCO/C2 image with an MLSO/MK4 image overlaid in the range  $1.1 - 2.2 R_{\odot}$ , dated 8 March 2011 at 20:24 and 20:22 UT respectively. The C2 image has been processed via the CORIMP techniques of normalizing radial graded filter (NRGF) and quiescent background subtraction. It has been trimmed to a half-width of  $3.4 R_{\odot}$ , which is the upper limit of the *PROBA2/SWAP* field-of-view as indicated by the dashed circle. The SWAP field-of-view during nominal operations is indicated by the dashed box. The *SDO/AIA* field-of-view is indicated by the inner dotted box. The limb of the Sun behind the occulter is indicated by the solid white circle. A CME is observed off the south-west limb as a bright loop structure with some inner core material, as seen here in the Thomson-scattered white-light coronagraph images. It is clear how the SWAP and AIA images can be used to bridge CME observations to the low corona and solar disk, for gaining insight to their initiation phase.

## 2. Observations & Techniques

Methods of multiscale image processing have been developed in recent years for use on coronagraph images to enhance the underlying structure. The fundamental idea behind these methods is to highlight details apparent on different scales within the data. Therefore, multiscale techniques provide an ability to remove small-scale features in images, essentially suppressing the noise such that the structures of interest can be revealed in greater detail. By applying them to coronagraph images, the morphology of CMEs as they propagate through the corona in a sequence of observations can be determined with better accuracy than previously possible (Byrne *et al.*, 2009, 2012).

These methods are now demonstrated for use on the MK4 coronagraph and SWAP EUV imager, to provide insight to the low-coronal morphology of erupting structures that may form CMEs. Details on the fundamental technique are outlined in Young and Gallagher (2008) wherein the magnitude of the multiscale gradient is used to show the relative strength of the detected edges in the image structure at a particular scale of the multiscale decomposition (i.e., the strongest edges appear brightest). To increase the signal-to-noise ratio of the edge detec-

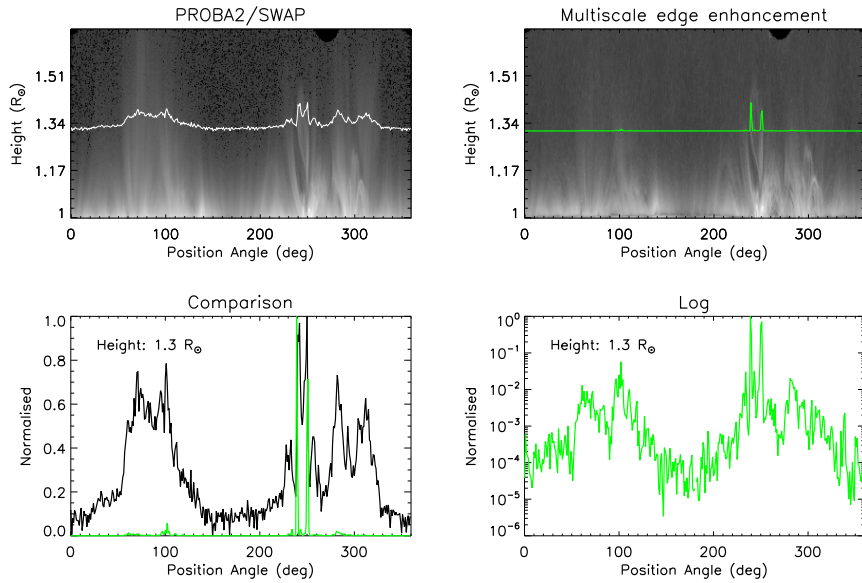


**Figure 2.** The top two panels show polar-unwrapped images of the solar corona across the *PROBA2/SWAP* field-of-view on 8 March 2011 at 19:53:59 UT; left being the level-1 data, right being the enhanced data. Across each image, at a constant height of  $1.3 R_\odot$ , an intensity slice is plotted (of arbitrary normalised units) to demonstrate how the background coronal structure is suppressed by the multiscale techniques, to highlight only the complex structure of the prominence. The bottom left plot shows a direct comparison of the two intensity slices, where the prominence is located between  $230 - 260^\circ$ . The bottom right plot shows a log scale of the normalised intensity slice across the enhanced image to demonstrate that the rest of the coronal structure is still present, just strongly suppressed relative to the prominence material.

tions further, the magnitude information from the scales most relevant to the coronal structures of interest may be multiplied together, neglecting the largest scales that smooth out the coronal signal, and the smallest scales that reveal the finer structure and noise (see Byrne *et al.*, 2012, for details). Thus the magnitude of the multiscale gradient across the dominant edges of coronal loops and CMEs is further enhanced for subsequent characterization of their morphology.

Figure 2 shows the effectiveness of the multiscale techniques for detecting the structure of an ejection observed by SWAP at 19:53:59 UT on 8 March 2011. The top left image shows the level-1 processed data, polar-unwrapped about Sun-center at coronal heights of  $1 - 1.7 R_\odot$ . The top right image shows the result of the multiscale filtering technique applied in such a manner as to enhance the edges of the detected structure in the data. The bottom left plot shows the comparison of an intensity slice at a height of  $1.3 R_\odot$  in each, revealing how the multiscale techniques best characterize the complex structure of the erupting prominence material. While the bottom right plot shows a log of the intensity slice across the multiscale filtered image to reveal the suppressed signal of the background features.

The extended corona from  $\sim 2 - 30 R_\odot$  is often observed with the Large Angle Spectrometric Coronagraph (LASCO; Brueckner *et al.*, 1995) onboard the

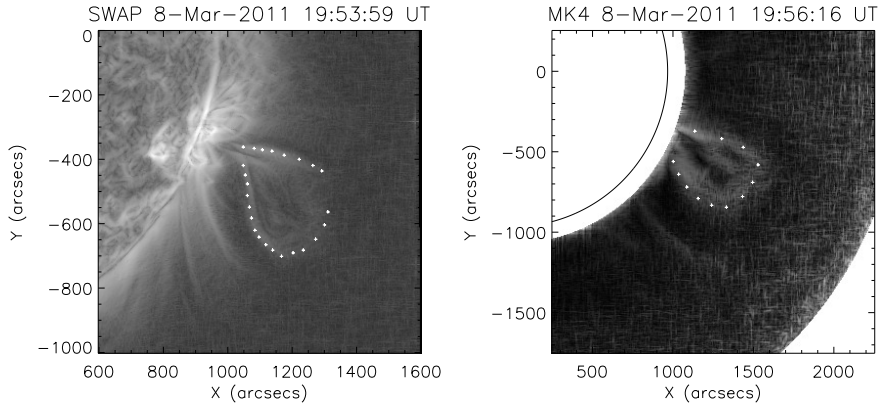


**Figure 3.** SWAP (left) and MK4 (right) observations of the erupting loop system that forms the inner core of the CME on 8 March 2011, at times 19:52 and 19:53 UT respectively. The images have been processed via the multiscale decomposition, showing here intensities that represent the magnitude of the detected edges.

Solar and Heliospheric Observatory (SOHO; Domingo, Fleck, and Poland, 1995) situated about the L1 point. (Along with the more recently launched SECCHI coronagraphs onboard the STEREO mission, from increasing angles of separation in their orbits about the Sun.) Coronal structures, and specifically CMEs, have been studied in the white-light image data from these instruments through the use of a number of steps outlined in the Coronal Image Processing package (CORIMP; Morgan, Byrne, and Habbal, 2012, Byrne *et al.*, 2012). These techniques have now been extended for use on the MLSO/MK4 coronagraph data, which provides white-light polarization brightness images of the corona from  $\sim 1.14 - 2.86 R_{\odot}$ . The MK4 data is prepared via an instrumental vignetting function that maximizes the image contrast by offsetting the radial brightness gradient in order to best reveal structures such as CMEs and streamers. A multiscale decomposition is then performed, in order to produce magnitude images of the relative edge strengths in the image to highlight the detected structure (see Fig. 3).

### 3. ‘Double Eruption’ of the 8 March 2011 CME

A CME erupted from active region NOAA 11165 (S20W91) at approximately 19:30 UT on 8 March 2011. The active region caused numerous flares during its evolution across the disk, notably an M1.5 flare at GOES start-time 19:35 UT associated with the rising loop system that erupted to form the core material of the CME. The loop system evolution is clearly visible up to  $\sim 1.3 R_{\odot}$  in *SDO/AIA* images, with the proceeding eruption observed to a height of  $\sim 1.6 R_{\odot}$  in the larger field-of-view of the *PROBA2/SWAP* imager. The CME core is then observed in the white-light MK4 coronagraph image data to a height of  $\sim 2.2 R_{\odot}$ , entrained within a very faint CME bubble that appears to form at these heights

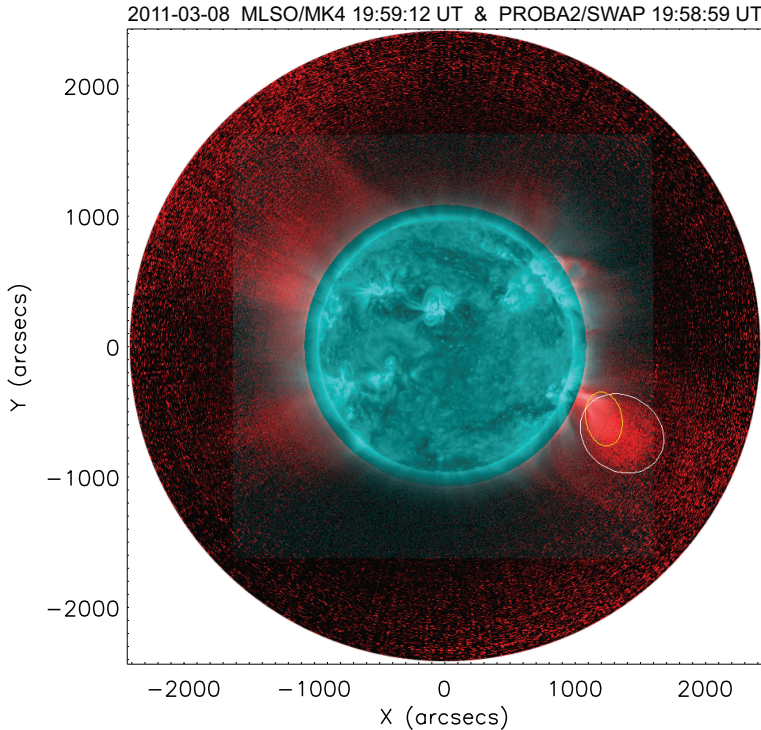


**Figure 4.** A merged SWAP (blue) and MK4 (red) image with the ellipse fits to the characterized CME core material as observed by each instrument.

before being clearly observed to propagate outwards in the extended LASCO/C2 and C3 coronagraph images (Fig. ??).

In order to best reveal the eruption material in the low signal-to-noise SWAP and MK4 images, multiscale methods of noise suppression and edge enhancement were employed, as discussed above. This allowed a point-&-click characterization of the core material of the CME, which was the brightest structure to be tracked through the different imagers when the CME front was not yet fully formed. Figure 3 shows example SWAP and MK4 magnitude (edge strength) images of the erupting structure. The rising loop system observed with SWAP, and the erupting CME core material observed with MK4 that coincided both temporally and spatially with the rising loops, at least initially, were characterized by ellipse-fits to the detected front edges of the structures. Figure 4 shows an overlay of a SWAP and MK4 images during the eruption at times 19:58:59 and 19:59:12 UT respectively, with the ellipses fit to the erupting fronts at those times (from point-&-click characterizations of the edge enhanced multiscale decompositions of the images, as demonstrated in Fig. 3). Figure 5 shows the progression of the ellipse fits to the fronts over the course of the eruption, indicating how the white-light material observed in MK4 propagates away from the source quicker than the EUV material observed in SWAP. The different height-time profiles of the SWAP and MK4 observations are shown in Fig. 6, where the material in the MK4 images attains a speed in the range  $\sim 400 - 600 \text{ km s}^{-1}$ , while the associated

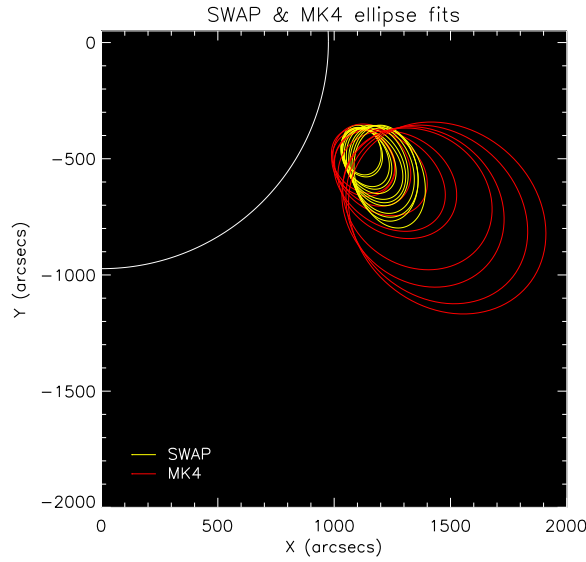


**Figure 5.** The SWAP and MK4 ellipse fits to the characterized CME core material over the course of the eruption.

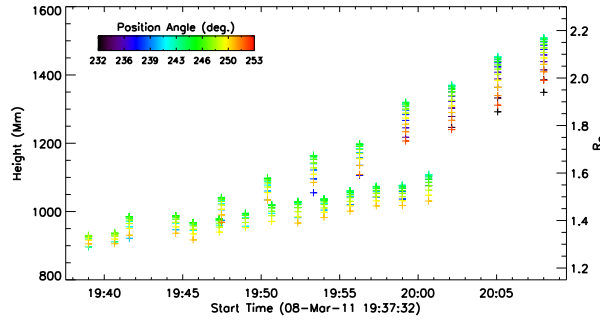


**Figure 6.** The ‘double eruption’ height-time profile of the characterized eruption observed simultaneously with the SWAP imager and MK4 coronagraph (see the ellipse-fits in Fig. ?? above). The erupting EUV loops move at a speed of  $\sim 100 \text{ km s}^{-1}$  while the associated core of the resulting CME is observed to accelerate up to a speed of  $\sim 400 \text{ km s}^{-1}$ .

erupting loop structures in the SWAP images proceed at only  $\sim 100 \text{ km s}^{-1}$ . . The reasons for this are unclear, but the analysis of Su *et al.* (2012) shows that the active region underwent a two-stage flaring process at the time of the eruption that is evidence for secondary heating (Fig. 8), which may underly a double eruption mechanism that explains the CME observations.

The CME onset was observed as a series of rising loops, that attained an initial steady height in the low corona of approximately half a solar radii, before destabilizing and becoming the inner core material of a typical three-part CME that propagated out through the corona at a bulk speed of  $\sim 400 \text{ km s}^{-1}$ , following an initial acceleration of  $\sim 20 \text{ m s}^{-2}$  away from the sun (based on the

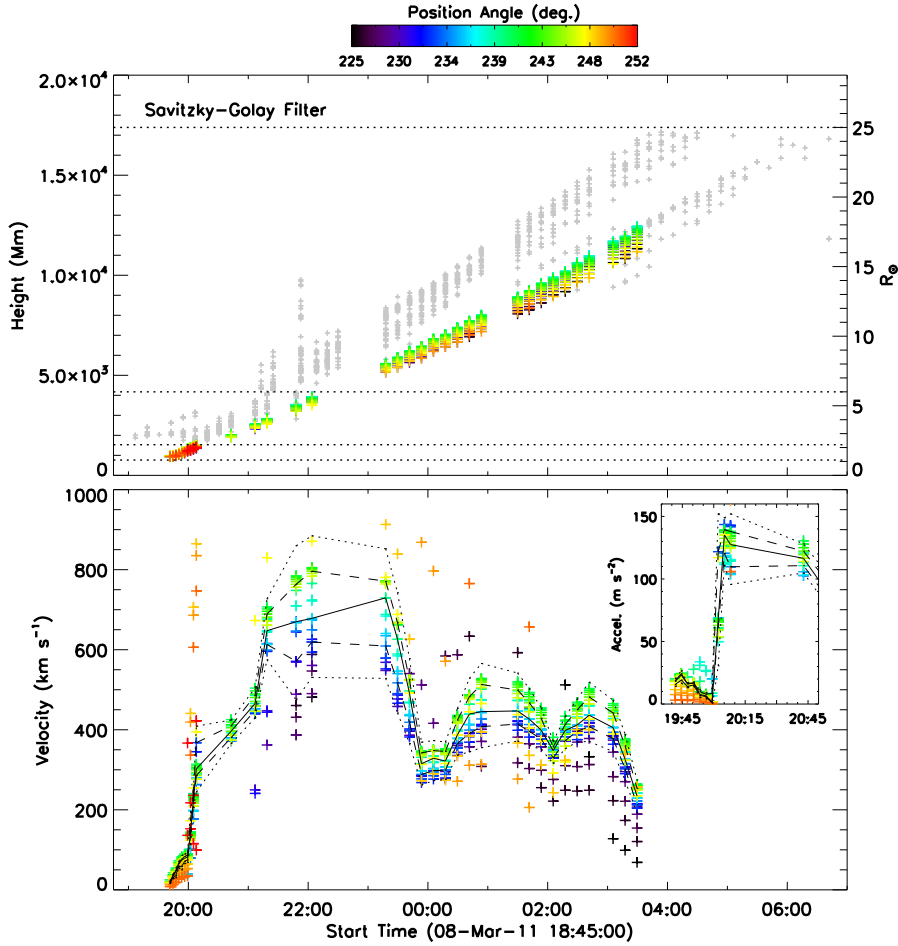


**Figure 7.**

kinematics of the CME front as detected and tracked in the CORIMP catalog<sup>1</sup>). The core of the CME was manually tracked via the multiscale methods and ellipse-fit discussed above, and the resulting kinematics are plotted in Fig. 7. The height-time profile of the CME core is shown in color (corresponding to the position angle of the measurements across the plane-of-sky) overlaid on the CME front height-time profiles shown in gray for comparison. The Savitzky-Golay filter is used to derive the velocity and acceleration profiles for the CME core (see Byrne *et al.*, 2013 for detailed discussion). A distribution of velocity and acceleration values is obtained at each data point, with the corresponding median, interquartile range, and upper and lower fences overlaid on each profile

<sup>1</sup><http://dublin.ifa.hawaii.edu/~jbyrne/CORIMP/>

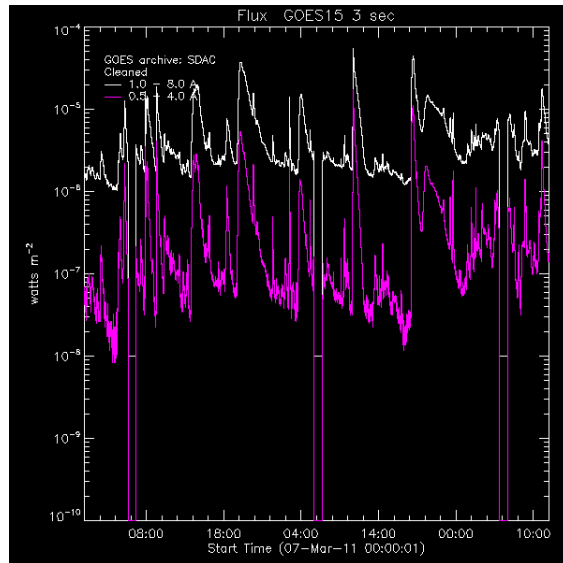


**Figure 8.** GOES x-ray flux profile in the lead-up to the rising loop system and ‘double eruption’ CME. The two-stage flare is visible just after 19:00 UT on 8 March 2011, being the M1.5 flare from NOAA AR 11165.

as solid, dashed and dotted lines respectively. The inset acceleration phase of the CME core shows an initial acceleration of approximately  $\sim 20 \text{ m s}^{-2}$  jumping to  $\sim 130 \text{ m s}^{-2}$ , which is in agreement with the acceleration profile of the CME front ahead of it. This double acceleration profile is further evidence of a two-stage solar eruptive event, as indicated by the differing height-time trends of Fig. 6 and the previous flare analysis of Su *et al.* (2012).

#### 4. Conclusions

**Acknowledgements** This work is supported by SHINE grant 0962716 and NASA grants NNX08AJ07G and NNX13AG11G to the Institute for Astronomy.

SWAP is a project of the Centre Spatial de Liège and the Royal Observatory of Belgium funded by the Belgian Federal Science Policy Office (BELSPO).

MK4 data is provided courtesy of the Mauna Loa Solar Observatory, operated by the High Altitude Observatory, as part of the National Center for Atmospheric Research (NCAR). NCAR is supported by the National Science Foundation.

#### References

- Brueckner, G.E., Howard, R.A., Koomen, M.J., Korendyke, C.M., Michels, D.J., Moses, J.D., Socker, D.G., Dere, K.P., Lamy, P.L., Llebaria, A., Bout, M.V., Schwenn, R., Simnett, G.M., Bedford, D.K., Eyles, C.J.: 1995, The Large Angle Spectroscopic Coronagraph (LASCO). *Solar Physics* **162**, 357–402. doi:10.1007/BF00733434.  
 Byrne, J.P., Gallagher, P.T., McAteer, R.T.J., Young, C.A.: 2009, The kinematics of coronal mass ejections using multiscale methods. *Astronomy & Astrophysics* **495**, 325–334. doi:10.1051/0004-6361:200809811.

- Byrne, J.P., Morgan, H., Habbal, S.R., Gallagher, P.T.: 2012, Automatic Detection and Tracking of Coronal Mass Ejections. II. Multiscale Filtering of Coronagraph Images. *Astrophysical Journal* **752**, 145. doi:10.1088/0004-637X/752/2/145.
- Byrne, J.P., Long, D.M., Gallagher, P.T., Bloomfield, D.S., Maloney, S.A., McAtee, R.T.J., Morgan, H., Habbal, S.R.: 2013, Improved methods for determining the kinematics of coronal mass ejections and coronal waves. *Astronomy & Astrophysics* **557**, A96. doi:10.1051/0004-6361/201321223.
- Domingo, V., Fleck, B., Poland, A.I.: 1995, The SOHO Mission: an Overview. *Solar Physics* **162**, 1–2. doi:10.1007/BF00733425.
- Druckmüllerová, H., Morgan, H., Habbal, S.R.: 2011, Enhancing Coronal Structures with the Fourier Normalizing-radial-graded Filter. *Astrophysical Journal* **737**, 88. doi:10.1088/0004-637X/737/2/88.
- Elmore, D.F., Burkepile, J.T., Darnell, J.A., Lecinski, A.R., Stanger, A.L.: 2003, Calibration of a ground-based solar coronal polarimeter. In: Fineschi, S. (ed.) *Society of Photo-Optical Instrumentation Engineers (SPIE) Conference Series, Society of Photo-Optical Instrumentation Engineers (SPIE) Conference Series* **4843**, 66–75. doi:10.1117/12.459279.
- Gallagher, P.T., Young, C.A., Byrne, J.P., McAtee, R.T.J.: 2011, Coronal mass ejection detection using wavelets, curvelets and ridgelets: Applications for space weather monitoring. *Advances in Space Research* **47**, 2118–2126. doi:10.1016/j.asr.2010.03.028.
- Lemen, J.R., Title, A.M., Akin, D.J., Boerner, P.F., Chou, C., Drake, J.F., Duncan, D.W., Edwards, C.G., Friedlaender, F.M., Heyman, G.F., Hurlburt, N.E., Katz, N.L., Kushner, G.D., Levay, M., Lindgren, R.W., Mathur, D.P., McFeaters, E.L., Mitchell, S., Rehse, R.A., Schrijver, C.J., Springer, L.A., Stern, R.A., Tarbell, T.D., Wuelser, J.-P., Wolfson, C.J., Yanari, C., Bookbinder, J.A., Cheimets, P.N., Caldwell, D., Deluca, E.E., Gates, R., Golub, L., Park, S., Podgorski, W.A., Bush, R.I., Scherrer, P.H., Gummin, M.A., Smith, P., Auker, G., Jerram, P., Pool, P., Soufli, R., Windt, D.L., Beardsley, S., Clapp, M., Lang, J., Waltham, N.: 2012, The Atmospheric Imaging Assembly (AIA) on the Solar Dynamics Observatory (SDO). *Solar Physics* **275**, 17–40. doi:10.1007/s11207-011-9776-8.
- Lockwood, M., Hapgood, M.: 2007, The Rough Guide to the Moon and Mars. *Astronomy and Geophysics* **48**(6), 060000–6. doi:10.1111/j.1468-4004.2007.48611.x.
- Morgan, H., Byrne, J.P., Habbal, S.R.: 2012, Automatically Detecting and Tracking Coronal Mass Ejections. I. Separation of Dynamic and Quiescent Components in Coronagraph Images. *Astrophysical Journal* **752**, 144. doi:10.1088/0004-637X/752/2/144.
- Morgan, H., Habbal, S.R., Woo, R.: 2006, The Depiction of Coronal Structure in White-Light Images. *Solar Physics* **236**, 263–272. doi:10.1007/s11207-006-0113-6.
- Pérez-Suárez, D., Higgins, P.A., Bloomfield, D.S., McAtee, R.T.J., Krista, L.D., Byrne, J.P., Gallagher, P.T.: 2011, "Automated Solar Feature Detection for Space Weather Applications", in *Applied Signal and Image Processing: Multidisciplinary Advancements*, eds. R. Qahwaji, R. Green, & E. L. Hines, (IGI Global), p. 207–225.
- Pesnell, W.D., Thompson, B.J., Chamberlin, P.C.: 2012, The Solar Dynamics Observatory (SDO). *Solar Physics* **275**, 3–15. doi:10.1007/s11207-011-9841-3.
- Santandrea, S., Gantois, K., Strauch, K., Teston, F., Tilmans, E., Baijot, C., Gerrits, D., De Groof, A., Schwemmer, G., Zender, J.: 2013, PROBA2: Mission and Spacecraft Overview. *Solar Physics* **286**, 5–19. doi:10.1007/s11207-013-0289-5.
- Schwenn, R., dal Lago, A., Huttunen, E., Gonzalez, W.D.: 2005, The association of coronal mass ejections with their effects near the Earth. *Annales Geophysicae* **23**, 1033–1059.
- Seaton, D.B., Berghmans, D., Nicula, B., Halain, J.-P., De Groof, A., Thibert, T., Bloomfield, D.S., Raftery, C.L., Gallagher, P.T., Auchère, F., Defise, J.-M., D'Huys, E., Lecat, J.-H., Mazy, E., Rochus, P., Rossi, L., Schühle, U., Slemzin, V., Yalim, M.S., Zender, J.: 2013, The SWAP EUV Imaging Telescope Part I: Instrument Overview and Pre-Flight Testing. *Solar Physics* **286**, 43–65. doi:10.1007/s11207-012-0114-6.
- Stenborg, G., Cobelli, P.J.: 2003, A wavelet packets equalization technique to reveal the multiple spatial-scale nature of coronal structures. *Astronomy & Astrophysics* **398**, 1185–1193. doi:10.1051/0004-6361:20021687.
- Stenborg, G., Vourlidas, A., Howard, R.A.: 2008, A Fresh View of the Extreme-Ultraviolet Corona from the Application of a New Image-Processing Technique. *Astrophysical Journal* **674**, 1201–1206. doi:10.1086/525556.
- Su, Y., Dennis, B.R., Holman, G.D., Wang, T., Chamberlin, P.C., Savage, S., Veronig, A.: 2012, Observations of a Two-stage Solar Eruptive Event (SEE): Evidence for Secondary Heating. *Astrophysical Journal Letters* **746**, L5. doi:10.1088/2041-8205/746/1/L5.

SWAP

---

- Yashiro, S., Gopalswamy, N., Michalek, G., St. Cyr, O.C., Plunkett, S.P., Rich, N.B., Howard, R.A.: 2004, A catalog of white light coronal mass ejections observed by the SOHO spacecraft. *Journal of Geophysical Research (Space Physics)* **109**, 7105. doi:10.1029/2003JA010282.
- Young, C.A., Gallagher, P.T.: 2008, Multiscale Edge Detection in the Corona. *Solar Physics* **248**, 457–469. doi:10.1007/s11207-008-9177-9.

